Journal of Computational Mathematics
Vol.31, No.5, 2013, 439–448.

http://www.global-sci.org/jcm
doi:10.4208/jcm.1304-m4388

A LOW-FREQUENCY ELECTROMAGNETIC NEAR-FIELD INVERSE PROBLEM FOR A SPHERICAL SCATTERER*

Nikolaos L. Tsitsas
Department of Informatics, Aristotle University of Thessaloniki, Thessaloniki, Greece
Email: ntsitsas@csd.auth.gr

Abstract

The interior low-frequency electromagnetic dipole excitation of a dielectric sphere is utilized as a simplified but realistic model in various biomedical applications. Motivated by these considerations, in this paper, we investigate analytically a near-field inverse scattering problem for the electromagnetic interior dipole excitation of a dielectric sphere. First, we obtain, under the low-frequency assumption, a closed-form approximation of the series of the secondary electric field at the dipole's location. Then, we utilize this derived approximation in the development of a simple inverse medium scattering algorithm determining the sphere's dielectric permittivity. Finally, we present numerical results for a human head model, which demonstrate the accurate determination of the complex permittivity by the developed algorithm.

Mathematics subject classification: 34L25, 78A46, 78A40, 41A60, 33C05.
Key words: Near-field inverse problems, Low-frequency region, Dipoles, Hypergeometric functions.

1. Introduction

The exact field solutions of direct scattering problems by canonical shapes are often expressed by complicated series of the corresponding eigenfunctions [1,2]. For example, for spherical scatterers the fields are expressed by series of products of spherical Bessel and Hankel functions. In inverse scattering these series are difficult to manipulate in order to obtain algorithms which extract a specific set of the problem's parameters. However, under the low-frequency assumption $k_0 a \ll 1$ (k_0 the free-space wavenumber and a a characteristic dimension of the scatterer) [3]- [6], the field solutions are greatly simplified so that the low-frequency realm offers a better environment for inverse scattering, since the corresponding field quantities are much more workable.

In this paper, we investigate analytically a near-field inverse scattering problem concerning the low-frequency interior dipole excitation of a dielectric sphere. The low-frequency assumption permits us to obtain an analytical expression, via hypergeometric functions, of the secondary electric field at the dipole's location by exact summation of the series representing it. This problem is motivated by potential applications considered in the low-frequency region and mentioned below.

Applications of low-frequency internal source excitation of a homogeneous sphere in electroencephalography (EEG) have been pointed out in [7]. In particular, the interior excitation of a spherical human head by a low-frequency point-dipole constitutes a suitable EEG model

* Received December 21, 2012 / Revised version received February 25, 2013 / Accepted April 16, 2013 / Published online August 27, 2013 /

(e.g., according to [8], $k_0 a \simeq 1.3 \times 10^{-7}$ for $f = 60$ Hz and head's radius $a = 10$ cm). Besides, magnetic resonance imaging low-frequency applications are discussed in [9] for a spherical head with $k_0 a \simeq 2 \times 10^{-6}$. A brain electrical impedance tomography low-frequency model with $k_0 a \simeq 1.9 \times 10^{-4}$ is investigated in [10]. Other applications stem from antennas implanted inside the head for hyperthermia or biotelemetry [11, 12]. For extensive reviews on using dipoles inside spheres for brain imaging applications see [13] and [14].

Far-field inverse scattering algorithms in the low-frequency region were established in [15] for acoustic scattering by a homogeneous sphere, due to an exterior point-source incident field, by utilizing essentially the distance of the source from the scatterer. Besides, for the point-source or point-dipole excitation of a layered sphere the exact Green's function, the far-field low-frequency approximations, and related far-field inverse scattering algorithms were given in [16] for acoustic and in [17] for electromagnetic waves. Far-field inverse problems, using low-frequency plane waves impinging on a soft sphere, were analyzed in [18]. The identification of small dielectric inhomogeneities from scattering amplitude measurements was investigated in [19]- [22].

The inverse problems, investigated in [15]- [19], are based on far-field measurements. The benefits of using the near-field quantity of the scattered field at the dipole point, in the development of inverse scattering algorithms for a perfectly conducting sphere excited by an exterior dipole have been pointed in [23]. Other implementations of near-field inverse problems are treated in [24] and [25, p. 133]. On the other hand, in [26] near-field inverse problems are analyzed concerning the determination of static point-sources and point-dipoles as well as acoustic point-sources located inside a homogeneous sphere. The inversion algorithms established in [26] use the moments obtained by integrating the product of the total field on the sphere's surface with spherical harmonic functions. Moreover, currents inside three-shell spherical models are determined by electro-magneto-encephalography measurements in [27].

This paper is organized as follows. In Section 2, we present the mathematical formulation of the interior dipole excitation problem of a dielectric sphere. In Section 3, we first summarize basic results concerning the exact Green's function of this excitation problem, and then derive the exact expression of the near-field quantity of interest, which is the secondary electric field at the dipole's location. Then, under the low-frequency assumption $k_0 a \ll 1$ (the sphere's radius, a, being much smaller than the wavelength of the primary field), we express analytically, via hypergeometric functions, the secondary electric field at the dipole's point by exact summation of its series. This result is utilized in Section 4 for the development of a simple inverse medium scattering algorithm for the determination of the sphere's complex permittivity. The developed algorithm utilizes the single measurement of the secondary electric field at the dipole point, which is located in the interior of the sphere, in order to formulate a non-linear equation the solution of which is the sphere's dielectric permittivity. Finally, in Section 5, we present numerical results concerning: (i) the convergence of the low-frequency to the exact electric field at the dipole's location, and (ii) the determination of the complex permittivity by the developed algorithm; the complex permittivity's value under determination is selected according to a widely used human head model [28].

2. Mathematical Formulation

Consider a spherical scatterer of radius a. The interior V_1 of the scatterer is homogeneous and is characterized by complex dielectric permittivity ϵ_1 and magnetic permeability

μ_1. The sphere's exterior V_0 is a homogeneous medium with physical constants ϵ_0 and μ_0 and wavenumber $k_0 = \omega(\epsilon_0\mu_0)^{1/2}$, where ω is the angular frequency. The scatterer is excited by a time-harmonic [$\exp(-i\omega t)$ time dependence] primary spherical electromagnetic wave, generated by an internal magnetic dipole located at r_1 of V_1 (i.e. $r_1 < a$) with dipole moment $\hat{\mathbf{y}}$. The respective primary electric field is given by:

$$\mathbf{E}^{pr}(\mathbf{r}) = \nabla \times \left(\frac{h_0(k_1|\mathbf{r}-\mathbf{r}_1|)}{ik_1 h_0(k_1 r_1)} \hat{\mathbf{y}} \right), \quad \mathbf{r} \in \mathbb{R}^3 \setminus \{\mathbf{r}_1\}, \tag{2.1}$$

where $r_1 = |\mathbf{r}_1|$, while $h_0(x) = \exp(ix)/(ix)$ denotes the zeroth-order spherical Hankel function of the first kind, and $k_1 = \omega(\epsilon_1\mu_1)^{1/2}$ the wavenumber of V_1.

The total electric field in V_0 is denoted by $\mathbf{E}^0$. By applying Sommerfeld's method (see e.g. [29], Section 6.32 and [30], Section 9.28; also known as the scattering superposition method in the terminology of [31]), the total electric field $\mathbf{E}^1$ in V_1 is defined as the superposition of the primary and the secondary field:

$$\mathbf{E}^1(\mathbf{r}) = \mathbf{E}^{pr}(\mathbf{r}) + \mathbf{E}^{sec}(\mathbf{r}), \quad \mathbf{r} \in V_1 \setminus \{\mathbf{r}_1\}. \tag{2.2}$$

The corresponding boundary value problem consists in determining the fields $\mathbf{E}^0 \in (\mathcal{C}^2(V_0) \cap \mathcal{C}^1(\overline{V_0}))^3$ and $\mathbf{E}^{sec} \in \left(\mathcal{C}^2(V_1) \cap \mathcal{C}^1(\overline{V_1})\right)^3$ satisfying the vector Helmholtz equations:

$$\left.\begin{aligned} \nabla^2\mathbf{E}^0(\mathbf{r}) + k_0^2\,\mathbf{E}^0(\mathbf{r}) &= \mathbf{0}, \quad \mathbf{r} \in V_0 \\ \nabla^2\mathbf{E}^{sec}(\mathbf{r}) + k_1^2\,\mathbf{E}^{sec}(\mathbf{r}) &= \mathbf{0}, \ \mathbf{r} \in V_1 \end{aligned}\right\}, \tag{2.3}$$

as well as the transmission boundary conditions on the scatterer's surface $r = a$:

$$\left.\begin{aligned} \hat{\mathbf{r}} \times \mathbf{E}^0(\mathbf{r}) - \hat{\mathbf{r}} \times \mathbf{E}^{sec}(\mathbf{r}) &= \hat{\mathbf{r}} \times \mathbf{E}^{pr}(\mathbf{r}) \\ \mu_r\,\hat{\mathbf{r}} \times \nabla \times \mathbf{E}^0(\mathbf{r}) - \hat{\mathbf{r}} \times \nabla \times \mathbf{E}^{sec}(\mathbf{r}) &= \hat{\mathbf{r}} \times \nabla \times \mathbf{E}^{pr}(\mathbf{r}) \\ \hat{\mathbf{r}} \cdot \mathbf{E}^0(\mathbf{r}) - \epsilon_r\,\hat{\mathbf{r}} \cdot \mathbf{E}^{sec}(\mathbf{r}) &= \epsilon_r\,\hat{\mathbf{r}} \cdot \mathbf{E}^{pr}(\mathbf{r}) \end{aligned}\right\}, \quad r = a, \tag{2.4}$$

where $\epsilon_r = \epsilon_1/\epsilon_0$ and $\mu_r = \mu_1/\mu_0$ are the relative dielectric permittivity and magnetic permeability of V_1 respectively.

Besides, the total field $\mathbf{E}^0$ in the unbounded domain V_0 must satisfy the Silver-Müller radiation condition [25]:

$$\lim_{r\to\infty} \left[\ \hat{\mathbf{r}} \times \nabla \times \mathbf{E}^0(\mathbf{r}) + ik_0 r \mathbf{E}^0(\mathbf{r})\ \right] = \mathbf{0}, \tag{2.5}$$

uniformly for all directions $\hat{\mathbf{r}} \in S^2 = \{\mathbf{x} \in \mathbb{R}^3, ||\mathbf{x}|| = 1\}$.

3. Direct Scattering Problem

The direct scattering problem concerns the determination of the electric fields $\mathbf{E}^0$ and $\mathbf{E}^{sec}$, satisfying (2.3)-(2.5), for known scatterer's geometry, material parameters and primary field given by (2.1).

3.1. Exact solution

The exact solution of the direct scattering problem is determined by applying the analytic algorithm described in [17]. In particular, the primary and secondary electric fields are represented by series of the spherical vector wave functions, and the unknown coefficients in the secondary field's expansions are determined by imposing the transmission boundary conditions (2.4) on the scatterer's surface.

We select the spherical coordinate system (r, θ, ϕ) with the origin O at the centre of the spherical scatterer and assume the magnetic dipole is located at $r = r_1$, $\theta = 0$. The primary spherical electric field is expressed as [17]:

$$\mathbf{E}^{pr}(\mathbf{r}) = \frac{i}{\hat{h}_0(k_1 r_1)} \begin{cases} \displaystyle\sum_{n=1}^{\infty} \frac{2n+1}{n(n+1)} \Big(\hat{\jmath}_n(k_1 r_1) \mathbf{N}^3_{e1n}(\mathbf{r}, k_1) - \hat{\jmath}'_n(k_1 r_1) \mathbf{M}^3_{o1n}(\mathbf{r}, k_1) \Big), & r > r_1, \\ \displaystyle\sum_{n=1}^{\infty} \frac{2n+1}{n(n+1)} \Big(\hat{h}_n(k_1 r_1) \mathbf{N}^1_{e1n}(\mathbf{r}, k_1) - \hat{h}'_n(k_1 r_1) \mathbf{M}^1_{o1n}(\mathbf{r}, k_1) \Big), & r < r_1, \end{cases} \tag{3.1}$$

where $\mathbf{M}^1_{o1n}$, $\mathbf{N}^1_{e1n}$, $\mathbf{M}^3_{o1n}$, and $\mathbf{N}^3_{e1n}$ are the spherical vector wave functions (see [32], (13.3.68)-(13.3.70)), while $\hat{\jmath}_n(z) = z\jmath_n(z)$ and $\hat{h}_n(z) = zh_n(z)$ are the Ricatti-Bessel functions, with $\jmath_n$ and h_n being the n^{th} order spherical Bessel and Hankel functions of the first kind; the prime denotes derivation with respect to the entire argument $k_1 r_1$.

The secondary electric fields in V_0 and V_1 are given by:

$$\mathbf{E}^{sec}(\mathbf{r}) = \frac{i}{\hat{h}_0(k_1 r_1)} \sum_{n=1}^{\infty} \frac{2n+1}{n(n+1)} \Big(\alpha_n \hat{h}_n(k_1 r_1) \mathbf{N}^1_{e1n}(\mathbf{r}, k_1) - \beta_n \hat{h}'_n(k_1 r_1) \mathbf{M}^1_{o1n}(\mathbf{r}, k_1) \Big), \qquad 0 < r < a, \tag{3.2}$$

$$\mathbf{E}^{0}(\mathbf{r}) = \frac{i}{\hat{h}_0(k_1 r_1)} \sum_{n=1}^{\infty} \frac{2n+1}{n(n+1)} \Big(\gamma_n \hat{h}_n(k_1 r_1) \mathbf{N}^3_{e1n}(\mathbf{r}, k_1) - \delta_n \hat{h}'_n(k_1 r_1) \mathbf{M}^3_{o1n}(\mathbf{r}, k_1) \Big), \qquad r > a. \tag{3.3}$$

The unknown coefficients α_n, β_n, γ_n, and δ_n are determined by imposing the boundary conditions (2.4) as:

$$\alpha_n = \frac{p_n}{w_n} \frac{\jmath_n(k_1 r_1)}{h_n(k_1 r_1)}, \quad \beta_n = \frac{q_n}{v_n} \frac{\hat{\jmath}'_n(k_1 r_1)}{\hat{h}'_n(k_1 r_1)}, \tag{3.4}$$

$$\gamma_n = \frac{1}{w_n} \frac{\jmath_n(k_1 r_1)}{h_n(k_1 r_1)}, \quad \delta_n = \frac{1}{v_n} \frac{\hat{\jmath}'_n(k_1 r_1)}{\hat{h}'_n(k_1 r_1)}, \tag{3.5}$$

where

$$w_n = -ik_1 a \sqrt{\epsilon_r \mu_r} \left(\jmath_n(k_1 a) \hat{h}'_n(k_0 a) - \epsilon_r^{-1} \hat{\jmath}'_n(k_1 a) h_n(k_0 a) \right), \tag{3.6}$$

$$p_n = -ik_1 a \sqrt{\epsilon_r \mu_r} \left(\epsilon_r^{-1} \hat{h}'_n(k_1 a) h_n(k_0 a) - h_n(k_1 a) \hat{h}'_n(k_0 a) \right), \tag{3.7}$$

$$v_n = -ik_1 a \left(\mu_r \jmath_n(k_1 a) \hat{h}'_n(k_0 a) - \hat{\jmath}'_n(k_1 a) h_n(k_0 a) \right), \tag{3.8}$$

$$q_n = -ik_1 a \left(\hat{h}'_n(k_1 a) h_n(k_0 a) - \mu_r h_n(k_1 a) \hat{h}'_n(k_0 a) \right). \tag{3.9}$$

In particular, for $\epsilon_r = \mu_r = 1$ (no interface at $r = a$), we can verify that $\mathbf{E}^0(\mathbf{r}) = \mathbf{E}^{pr}(\mathbf{r})$ and $\mathbf{E}^{sec}(\mathbf{r}) = \mathbf{0}$, as expected.

We will utilize the secondary electric field at the dipole's location in order to establish the inverse medium scattering algorithm detailed below. Since the dipole is located at $\theta = 0$, the spherical vector wave functions are reduced to:

$$\mathbf{N}^1_{e1n}(\mathbf{r}_1, k_1) = \frac{1}{2} n(n+1) \frac{\hat{\jmath}'_n(k_1 r_1)}{k_1 r_1} \hat{\mathbf{x}} \quad , \quad \mathbf{M}^1_{o1n}(\mathbf{r}_1, k_1) = \frac{1}{2} n(n+1) \jmath_n(k_1 r_1) \hat{\mathbf{x}}, \tag{3.10}$$

and hence this secondary electric field is expressed by means of (3.2) as:

$$\mathbf{E}^{sec}(\mathbf{r_1}) = \hat{\mathbf{x}} \frac{i}{2k_1 r_1 h_0(k_1 r_1)} \sum_{n=1}^{\infty} (2n+1) \Big(\alpha_n h_n(k_1 r_1) \hat{\jmath}'_n(k_1 r_1) - \beta_n \hat{h}'_n(k_1 r_1) \jmath_n(k_1 r_1) \Big). \tag{3.11}$$

3.2. Near-field low-frequency approximations

The exact Eq. (3.11) represents the electric field at the dipole's location by a series of terms involving products of spherical Bessel and Hankel functions. In inverse scattering this series expression is difficult to manipulate in order to extract the required problem's parameters. However, the low-frequency assumption simplifies the field expressions and makes them more workable for inverse scattering purposes. For these reasons in the sequel we impose the *low-frequency assumption* $k_0 a \ll 1$, that is we assume that the sphere's radius, a, is much smaller than the wavelength of the primary field. More precisely, we suppose that $k_0 a$, $k_1 a$, $k_0 r_1$, and $k_1 r_1$ are all small (the waves are long compared to all geometrical lengths [33]), whereas the relative material parameters k_1/k_0, ϵ_r, and μ_r need not be small. As discussed in the Introduction, the low-frequency assumption is motivated and justified by several representative applications (see [7–9, 13]).

In order to find the low-frequency approximation of the secondary electric field at the dipole's location (3.11), we need the following asymptotic expansions, as $k_1 r_1 \to 0$:

$$\hat{\jmath}'_n(k_1 r_1) h_n(k_1 r_1) \sim -\frac{i(n+1)}{(2n+1) k_1 r_1} \quad , \quad \jmath_n(k_1 r_1) \hat{h}'_n(k_1 r_1) \sim \frac{i\, n}{(2n+1) k_1 r_1}, \tag{3.12}$$

as well as the asymptotic approximations of the coefficients α_n and β_n of (3.4), as all $k_0 a$, $k_1 a$, $k_0 r_1$, and $k_1 r_1 \to 0$:

$$\alpha_n \sim (1 - \epsilon_r) \frac{n}{n\epsilon_r + n + 1} \tau^{2n+1} \quad , \quad \beta_n \sim (\mu_r - 1) \frac{n+1}{n\mu_r + n + 1} \tau^{2n+1}, \tag{3.13}$$

where

$$\tau \equiv r_1 / a \, < 1 \, . \tag{3.14}$$

By combining (3.11)-(3.14), we obtain the following low-frequency approximation of the secondary electric field at the dipole's location:

$$\mathbf{E}^{sec}(\mathbf{r_1}) \sim \hat{\mathbf{x}} \, \frac{i \exp(-ik_1 r_1)}{2k_1 r_1} \, \left[(1 - \epsilon_r) \mathcal{E}(\epsilon_r, \tau) - (1 - \mu_r) \mathcal{M}(\mu_r, \tau) \right], \tag{3.15}$$

where

$$\mathcal{E}(\epsilon_r, \tau) = \sum_{n=1}^{\infty} \frac{n(n+1)}{n\epsilon_r + n + 1} \tau^{2n+1} \quad , \quad \mathcal{M}(\mu_r, \tau) = \sum_{n=1}^{\infty} \frac{n(n+1)}{n\mu_r + n + 1} \tau^{2n+1}. \tag{3.16}$$

Eq. (3.15) indicates that the influence of the relative permittivity ϵ_r and the relative permeability μ_r on the secondary electric field is separated and described exclusively by the series $\mathcal{E}(\epsilon_r,\tau)$ and $\mathcal{M}(\mu_r,\tau)$, respectively. Moreover, we see that the leading-order term of $\mathbf{E}^{sec}(\mathbf{r_1})$ in Eq. (3.15) is $\mathcal{O}(\frac{1}{k_1 r_1})$, as $k_1 r_1 \to 0$. Also, every term in the infinite series $\mathcal{E}(\epsilon_r,\tau)$ and $\mathcal{M}(\mu_r,\tau)$ contributes to this leading-order term.

4. Inverse Medium Scattering Problem

The general description of an *inverse medium scattering problem* consists in evaluating the electromagnetic material parameters from the measurements of the scattered electromagnetic field due to known illuminations (see [25] and [34–36] and the related references cited).

In the present setting, the inverse medium scattering problem under consideration concerns the determination of the sphere's complex dielectric permittivity ϵ_r for known sphere's radius a and dipole's location r_1. The biomedical applications, discussed in the Introduction above, suggest that it is physically relevant to consider that $\mu_r = 1$; the case of $\mu_r \neq 1$ may be handled by similar procedures, nevertheless involving more complicated computations.

First, we manipulate appropriately the low-frequency expression (3.15) of the secondary electric field at the dipole's location in order for it to be cast into a suitable form for the establishment of an inverse medium scattering algorithm determining the sphere's permittivity. In particular, Eq. (3.15) implies that:

$$|\mathbf{E}^{sec}(\mathbf{r_1})| \sim \frac{1}{k_0 r_1}\frac{|1-\epsilon_r|}{2|\sqrt{\epsilon_r}|}\,|\mathcal{E}(\epsilon_r,\tau)|\,. \tag{4.1}$$

By means of the Gauss hypergeometric function ([37], (15.2.1) and (15.5.1)):

$$F(a,b;c;z) \equiv {}_2F_1(a,b;c;z) = \frac{\Gamma(c)}{\Gamma(a)\Gamma(b)}\sum_{s=0}^{\infty}\frac{\Gamma(a+s)\Gamma(b+s)}{\Gamma(c+s)s!}z^s\,,$$

where Γ denotes the gamma function, the series $\mathcal{E}(\epsilon_r,\tau)$ is written successively as follows:

$$\begin{aligned}\mathcal{E}(\epsilon_r,\tau) = \sum_{n=1}^{\infty}\frac{n(n+1)}{n\epsilon_r+n+1}\tau^{2n+1} &= \frac{\tau^2}{2}\gamma\frac{\partial}{\partial\tau}\left(\sum_{n=0}^{\infty}\frac{n+1}{n+\gamma}\tau^{2n}\right)\\ &= \frac{\tau^2}{2}\frac{\partial F(\gamma,2;\gamma+1;\tau^2)}{\partial\tau} = \frac{2\gamma\tau^3}{\gamma+1}F(\gamma+1,3;\gamma+2;\tau^2),\end{aligned} \tag{4.2}$$

where

$$\gamma = \frac{1}{1+\epsilon_r}\,. \tag{4.3}$$

Finally by combining Eqs. (4.1) and (4.2) we get:

$$|\mathbf{E}^{sec}(\mathbf{r_1})| \sim \frac{1}{k_0 r_1}\,\tau^3\left|\frac{2\gamma-1}{\gamma+1}\right|\left|\sqrt{\frac{\gamma}{1-\gamma}}\right||F(\gamma+1,3;\gamma+2;\tau^2)|. \tag{4.4}$$

Now, we formulate the following inverse medium scattering algorithm: (i) measure the modulus m of the low-frequency expansion of the secondary electric field at the dipole's location for known sphere's radius a and dipole's location r_1; (ii) determine the parameter γ (and hence

the relative dielectric permittivity ϵ_r of the sphere by (4.3)) as the solution of the following non-linear equation, resulting directly from (4.4):

$$\left|\frac{2\gamma-1}{\gamma+1}\right|\left|\sqrt{\frac{\gamma}{1-\gamma}}\right||F(\gamma+1,3;\gamma+2;r_1^2/a^2)| = m\,k_0 a\,\frac{a^2}{r_1^2}\,. \tag{4.5}$$

5. Numerical Results and Discussion

In this section, first, we investigate by numerical simulations the convergence of the low-frequency to the exact electric field at the dipole's location; the exact field is computed by means of (3.11), while the low-frequency one by (3.15). Then, we present results concerning the numerical determination of ϵ_r by means of (4.5).

Figs. 5.1 and 5.2 depict both the exact and low-frequency electric field modulus $|\mathbf{E}^{sec}(\mathbf{r_1})|$ as well as the relative error between the respective exact and low-frequency values, as functions of k_0a for $r_1 = a/2$ with $\epsilon_r = 2$ for Fig. 5.1 and $\epsilon_r = 6$ for Fig. 5.2. The convergence of the low-frequency to the exact field exhibits significant accuracy for a relatively wide range of k_0a. This fact is particularly important for the numerical implementation of the inverse medium scattering algorithm of section 4, which is essentially based on the low-frequency field's expansion (3.15). More precisely, as is expected, for $k_0a \ll 1$ the achieved convergence is excellent. Besides, good convergence is achieved also for certain k_0a lying outside the low-frequency regime. Hence, the derived low-frequency results of section 4.2 remain valid (to an appropriate approximation) for relatively small values of k_0a, which do not necessarily satisfy $k_0a \ll 1$. In particular, the values of k_0a for which the relative error between the exact and low-frequency fields is smaller than a certain threshold are indicated by the statements of Figs. 5.1b and 5.2b. For example, a relative error of 10% is obtained for $k_0a = 0.58$ when $\epsilon_r = 2$ and for $k_0a = 0.3$ when $\epsilon_r = 6$.

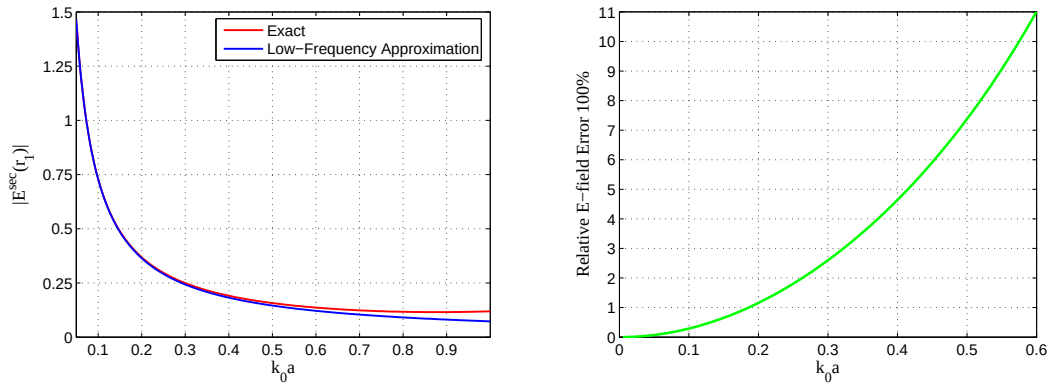

Fig. 5.1. (a) Exact and low-frequency electric field modulus $|\mathbf{E}^{sec}(\mathbf{r_1})|$, and (b) relative error between the exact and the low-frequency values of $|\mathbf{E}^{sec}(\mathbf{r_1})|$, both as functions of k_0a for $\epsilon_r = 2$ and $r_1 = a/2$.

Furthermore, Table 5.1 depicts the numerical results from the determination of ϵ_r by means of (4.5) for the case of the true value of ϵ_r being that corresponding to the complex permittivity of the IEEE head model [28]. The magnetic dipole is located at $r_1 = a/2$. The non-linear Eq. (4.5) is solved by means of the complex Müller's method. The latter is an iterative method based on the secant method, uses three points and constructs the parabola through these points in order to obtain the next approximation. Müller's method has gained a reputation as an efficient and fairly reliable method for finding a zero of a function defined on the complex

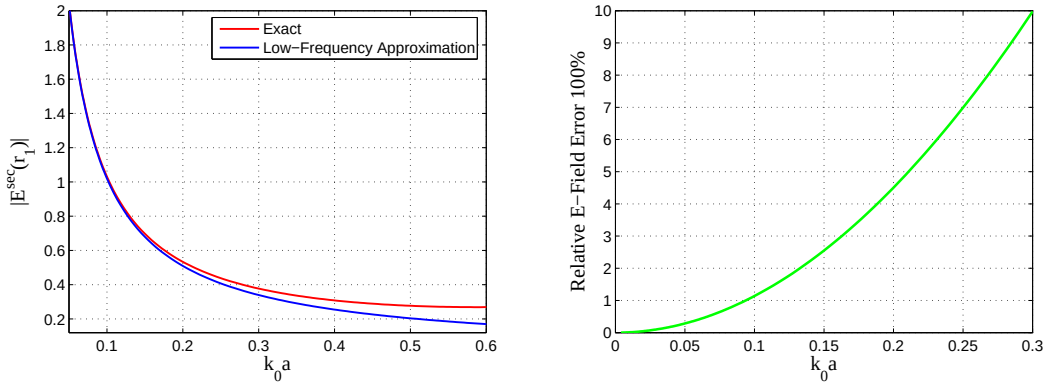

Fig. 5.2. The same with Fig. 5.1 but for $\epsilon_r = 6$.

Table 5.1: Numerical determination of ϵ_r as solution of the non-linear Eq. (4.5); the true value $\epsilon_r = 43.50 - 34.75\,i$ corresponds to the complex permittivity of the IEEE head model [28].

k_0a	0.05	0.01	0.001
True ϵ_r	$43.50 - 34.75\,i$	$43.50 - 34.75\,i$	$43.50 - 34.75\,i$
Reconstructed ϵ_r	$44.87 - 45.72\,i$	$43.94 - 36.72\,i$	$43.54 - 34.94\,i$
Relative Error $\Re[\epsilon_r]$ 100%	3%	1%	0.1%
Relative Error $\Im[\epsilon_r]$ 100%	30%	5%	0.5%

plane. In particular, the approximating sequence of this method may be complex even if the non-linear equation to be solved as well as the starting values are real. The method is implemented here as described in details in Section 5.9 of [38]. For the computations of Table 5.1 the initial vector, required by Müller's method, is $[33.6 - 15.7\,i,\ 25.7 - 8.6\,i, 20.4 - 5.3\,i]^{\mathrm{T}}$. Notice that the values of the initial vector are not chosen close to the value of the permittivity under determination.

Evidently, the approximation's accuracy in the determination of ϵ_r increases with decreasing k_0a; this is due to the fact that, as is shown in Figs. 5.1 and 5.2, the error in the approximation of the exact by the low-frequency electric field modulus $|\mathbf{E}^{sec}(\mathbf{r_1})|$ decreases with decreasing k_0a. We emphasize that in the low-frequency regime, where the inverse scattering algorithm is established, the obtained accuracy for the approximation of ϵ_r is indeed significant; for example for $k_0a = 0.001$ the relative errors in the determination of both the real and imaginary parts of ϵ_r are smaller than 1%. The significant error observed for $k_0a = 0.05$ is due to the fact that the accuracy in the approximation (4.4) decreases for increasing k_0a, namely as we move away from the low-frequency regime.

Aspects of the numerical determination of the complex permittivity ϵ_r for varying values of the problem's parameters involved are worthwhile to be investigated further as future work.

6. Conclusions

We investigated the inverse scattering problem of the interior dipole excitation of a homogeneous dielectric sphere. The exact Green's function of this problem was approximated in the

low-frequency region. The electric field at the interior dipole's location was expressed analytically by exact summation of the relevant series representing it. Then, we established a simple inverse medium scattering algorithm by utilizing the single measurement of the modulus of the secondary electric field at the dipole's location. More precisely, the unknown dielectric permittivity of the sphere was determined as the solution of a suitable non-linear equation. Numerical results were presented demonstrating the accurate determination of the complex permittivity by the developed algorithm for permittivity's value corresponding to a widely used human head model.

Appropriate modifications of the techniques of this paper may be applied to investigate in a similar way the excitation problem of a dielectric sphere by an exterior dipole. In this case the measurement data could be simpler to obtain.

Acknowledgments. The author would like to thank sincerely Prof. Paul A. Martin for various constructive discussions on this topic.

References

[1] J.J. Bowman, T.B. Senior, P.L. Uslenghi, Electromagnetic and Acoustic Scattering by Simple Shapes, North Holland Publ. Co., 1969.

[2] S.S. Vinogradov, P.D. Smith, E.D. Vinogradova, Canonical Problems in Scattering and Potential Theory, Part II, Chapman & Hall/CRC, 2002.

[3] G. Dassios and R. Kleinman, Low Frequency Scattering, Clarendon Press, 2000.

[4] H. Ammari and H. Kang, Reconstruction of Small Inhomogeneities from Boundary Measurements, Lecture Notes in Mathematics 1846, Springer-Verlag, 2004.

[5] H. Ammari and H. Kang, Boundary layer techniques for solving the Helmholtz equation in the presence of small inhomogeneities, *J. Math. Anal. Appl.*, **296** (2004), 190-208.

[6] H. Ammari, D. Volkov, M. Vogelius, Asymptotic formulas for perturbations in the electromagnetic fields due to the presence of inhomogeneities of small diameter II. The full Maxwell equations, *J. Math. Pures et Appl.*, **80** (2001), 769-814.

[7] J.C.E. Sten, I.V. Lindell, Electrostatic Image Theory for the Dielectric Sphere with an Internal Source, *Microw. Opt. Technol. Let.*, **5** (1992), 597-602.

[8] I.S. Koh, W.T. Kim, J.G. Yook, J.C. Park, Semi-analytical time-domain low-frequency scattering formulation for biological applications, *Int. J. Numer. Model.-Elec. Netw. Devic. and Fields*, **20** (2007), 93-108.

[9] F. Liu and S. Crozier, Electromagnetic fields inside a lossy, multilayered spherical head phantom excited by MRI coils: models and methods, *Phys. Medic. Biol.*, **49** (2004), 1835-1851.

[10] C.Y. Xiao and Y.Z. Lei, Analytical solutions of electric potential and impedance for a multilayered spherical volume conductor excited by time-harmonic electric current source: application in brain EIT, *Phys. Medic. Biol.*, **50** (2005), 2663-2674.

[11] J. Kim and Y. Rahmat-Samii, Implanted antennas inside a human body: Simulations, designs, and characterizations, *IEEE Trans. Microw. Th. Techniq.*, **52** (2004), 1934-1943.

[12] S.M.S. Reyhani and S. A. Ludwig, Implanted spherical head model for numerical EMC investigation, *Electromagnetics*, **25** (2005), 93-114.

[13] G. Dassios, Electric and magnetic activity of the brain in spherical and ellipsoidal geometry, *Lect. Notes in Math.*, **1983** (2009), 133-202.

[14] H. Ammari, An Introduction to Mathematics of Emerging Biomedical Imaging, Springer, 2008.

[15] G. Dassios and G. Kamvyssas, Point source excitation in direct and inverse scattering: the soft and the hard small sphere, *IMA J. Appl. Math.*, **55** (1995), 67-84.

[16] N.L. Tsitsas and C. Athanasiadis, Point-source excitation of a layered sphere: direct and far-field inverse scattering problems, *Quart. J. Mech. Appl. Math.*, **61** (2008), 549-580.
[17] N.L. Tsitsas, Direct and inverse dipole electromagnetic scattering by a piecewise homogeneous sphere, *Zeit. Angew. Math. Mech.*, **89** (2009), 833-849.
[18] X. Liu and B. Zhang, Unique determination of a sound-soft ball by the modulus of a single far field datum, *J. Math. Anal. Appl.*, **365** (2010), 619-624.
[19] H. Ammari, E. Iakovleva, S. Moskow, Recovery of Small Inhomogeneities from the Scattering Amplitude at a Fixed Frequency, *SIAM J. Math. Anal.*, **34** (2003), 882900.
[20] H. Ammari, E. Iakovleva, D. Lesselier, G. Perrusson, MUSIC-type electromagnetic imaging of a collection of small three-dimensional inclusions, *SIAM J. Sci. Comput.*, **29** (2007), 674-709.
[21] H. Ammari, E. Iakovleva, D. Lesselier, A MUSIC algorithm for locating small inclusions buried in a half-space from the scattering amplitude at a fixed frequency, *Multiscale Model. Simul.*, **3** (2005), 597-628.
[22] H. Ammari, H. Kang, E. Kim, J.Y. Lee, The generalized polarization tensors for resolved imaging. Part II: Shape and electromagnetic parameters reconstruction of an electromagnetic inclusion from multistatic measurements, *Math. Comput.*, **81** (2012), 839-860.
[23] C. Athanasiadis, P.A. Martin, I.G. Stratis, On the scattering of point-generated electromagnetic waves by a perfectly conducting sphere, and related near-field inverse problems, *Zeit. Angew. Math. Mech.*, **83** (2003), 129-136.
[24] C.J.S. Alves and P.M.C. Ribeiro, Crack detection using spherical incident waves and near-field measurements. *Boundary Elements XXI* (C. A. Brebbia, H. Power, eds.), WIT Press, Southampton. 1999, 355–364.
[25] D. Colton and R. Kress, Inverse acoustic and electromagnetic scattering theory, Springer, 1998.
[26] N.L. Tsitsas and P.A. Martin, Finding a source inside a sphere, *Inverse Problems*, **28** (2012), 015003.
[27] G. Dassios and A.S. Fokas, Electro-magneto-encephalography for a three-shell model: dipoles and beyond for the spherical geometry, *Inverse Problems*, **25** (2009), 035001.
[28] Evaluating Compliance With FCC Guidelines for Human Exposure to Radiofrequency Electromagnetic Fields, 9701 ed. Washington, DC: Federal Communication Commission (FCC) Std. Supplement C, OET Bulletin 65, 2001.
[29] A. Sommerfeld, Partial Differential Equations in Physics, Academic Press, 1949.
[30] J.A. Stratton, Electromagnetic Theory, McGraw-Hill, 1941.
[31] C.T. Tai, Dyadic Green Functions in Electromagnetic Theory, IEEE Press, 1994.
[32] P.M. Morse, and H. Feshbach, Methods of Theoretical Physics, McGraw-Hill, 1953.
[33] P.A. Martin, Multiple Scattering, Cambridge University Press, 2006.
[34] G. Bao, S. Hou, P. Li, Recent Studies on Inverse Medium Scattering Problems, *Modeling and Computations in Electromagnetics, Lecture Notes in Computational Science and Engineering*, **59** (2008).
[35] H. Ammari and H. Kang, Reconstruction of Small Inhomogeneities from Boundary Measurements, Lecture Notes in Mathematics 1846, Springer-Verlag, 2004.
[36] H. Ammari and H. Kang, Expansion Methods, Handbook of Mathematical Methods in Imaging, Springer, 2011 (447-499).
[37] F.W.J. Olver, D.W. Lozier, R.F. Boisvert, C.W. Clark (Eds.), NIST Handbook of Mathematical Functions, Cambridge University Press, 2010.
[38] J. Stoer and R. Bulirsch, Introduction to Numerical Analysis, Texts in Applied Mathematics 12, Springer, 2002.